Available online at www.sciencedirect.com
ScienceDirect
Journal of the European Ceramic Society 29 (2009) 2773–2781
www.elsevier.com/locate/jeurceramsoc

Loadable TiO_2 scaffolds—A correlation study between processing parameters, micro CT analysis and mechanical strength

G. Fostad [a,1], B. Hafell [a,1], A. Førde [a,1], R. Dittmann [b], R. Sabetrasekh [a], J. Will [c], J.E. Ellingsen [d], S.P. Lyngstadaas [a], H.J. Haugen [a,*]

[a] *Department for Biomaterials, Faculty for Odontology, University of Oslo, PO Box 1109 Blindern, NO-0317 Oslo, Norway*
[b] *Laboratory for High Performance Ceramics, EMPA Materials Science and Technology, Ueberlandstrasse 129, CH-8600 Duebendorf, Switzerland*
[c] *Institute of Glass and Ceramics, Department of Materials Science and Engineering, University of Erlangen-Nürnberg, Henkestr. 91, D-91052 Erlangen, Germany*
[d] *Oral Research Laboratory, Faculty for Odontology, University of Oslo, PO Box 1109 Blindern, NO-0317 Oslo, Norway*

Received 30 January 2009; received in revised form 19 March 2009; accepted 20 March 2009
Available online 24 April 2009

Abstract

It was shown in the present study that it is possible to produce TiO_2 scaffolds with both high mechanical strength and high porosity by using the polymer sponge method. TiO_2 scaffolds with porosity above 85% exceeded 1 MPa in compressive strength. TiO_2 scaffolds with equally high compressive strength having a fully open porosity close to 90% is not previously been reported in the literature. Reduction of porosity leads to even further reinforce the scaffolds' mechanical structure. A statistical correlation study with 160 tested scaffolds defined the most important manufacturing steps and the governing morphological characteristics for the scaffold's increased mechanical strength. The key manufacturing factors were a holding phase during sintering time for more than 30 h (at 1500 °C) and multiple coatings of the scaffold's structure. The crucial parameters for high mechanical strength were the fractal dimensions of the struts, object surface/volume ratio, density and overall porosity.

Keywords: Porosity; Microstructure; Strength; TiO_2; Biomedical applications

1. Introduction

Bone tissue engineering offers an alternative approach to the repair and regeneration of lost bone.[1] Scaffolds have become widely used in this field. The idea is that a well-constructed scaffold may let the human body reconstruct or replace damaged bone while providing a loadable structure during healing and function as a space keeper during the healing phase. Another important function of the scaffold is to serve as a framework for the cells when forming the tissue. The markets demand for having such a functional scaffolds is increasing[2] and there is not enough between available allogenic bone graft and people in need.[3] Reconstruction of bone defects caused by trauma, radiation, bone tumour removal or other bone disabling processes is also of major interest.

Different materials have been widely tested for making of scaffolds for use in bone tissue engineering.[4–9] Ideally, a scaffold for such purpose should have the following characteristics:

(1) three-dimensional and highly porous with an interconnecting pore network for cell growth and transport of nutrients and metabolic waste[10];
(2) biocompatible with either osseoconductive or osseoinductive properties[11–13];
(3) suitable surface chemistry for cell attachment, proliferation and differentiation;
(4) mechanical properties to match bone[13];
(5) suitable for industrial manufacturing and scale up.[13]

One strategy for regeneration of bone is the use of ceramic scaffolds that mimic the structure of bone mineral and that bind to bone; in some cases these ceramic scaffolds can activate the

* Corresponding author. Tel.: +47 22 85 23 50; fax: +47 22852351.
E-mail address: h.j.haugen@odont.uio.no (H.J. Haugen).
[1] These authors have contributed equal amount into the work and should therefore all be regarded as first author.

0955-2219/$ – see front matter © 2009 Elsevier Ltd. All rights reserved.
doi:10.1016/j.jeurceramsoc.2009.03.017

genes within bone cells to stimulate new bone growth.[13] A bone scaffold should have the ability to carry the load while bone growth is proceeding, usually over months and even years. It is thus the authors' belief that a non-resorbable material would provide a more predictable treatment outcome than observed with restorable scaffolds. Titanium oxide (TiO_2) was chosen as scaffold material in the present study since this material has proven to fulfil many of the demands for a scaffold material. TiO_2 has shown to be biocompatible,[14] enhance bone and vascular ingrowth[15] and to have a certain degree of bacteriostatic effect.[16,17] One of the major obstacle with bone scaffold is its function as load bearing device,[18–21] so also with TiO_2 scaffolds.

So far, state of the art three-dimensional scaffolds for tissue engineering purposes has yet to meet the mechanical requirement as they lack strength when produced with sufficient interconnected pores and porosity.[22–25] The main goal of this project was to improve mechanical properties of TiO_2 scaffolds.

2. Materials and methods

2.1. Slurry preparation and characterization

The ceramic slurry was prepared with 60 g of TiO_2 (Pharma FP Hobitam, Sachtleben GmbH, Duisburg, Germany) gradually added into 29.7 ml sterile water at the pH 1.7 under stirring at a low-rotation speed 1000 rpm (Dispermat Ca-40, VMA-Getzmann GmbH, Reichshof, Germany). The zeta potential was found by laser measurements (Zetasizer 2000, Malvern, Heggerberg, Germany). When the slurry was homogenous, the rotation speed of the dissolver was increased to 5000 rpm for 4 h. The TiO_2 powder was gradually added while the temperature was held at room temperature. When the rotation speed was increased to 5000 rpm, the slurry temperature was reduced to 15 °C.

Three different mills were compared; bead mill (Walzenmühle Multifix M865, Alfred Schwinherr, Schwäbisch-G., Germany), planetary mono mill (Pulverisette 6, Fritsch Laborgerätebau, Idar-Oberstein, Germany) and a high speed dissolver (Dispermat Ca-40, VMA-Getzmann GmbH, Reichshof, Germany) in terms of optimal particle size distribution. Particle size distribution of the ceramic slurry was determined by laser particle measurement (Analysette 22″-NanoTec, Fritsch GmbH, Idar-Oberstein, Germany). All samples were dispersed in water and had 30 s of ultrasonic treatment.

2.2. Preparation of TiO_2 scaffold

The scaffold was prepared by the polymer sponge method.[26] Fully reticulated polyester based polyurethane foams with 45 ppi (Bulbren S, Eurofoam GmbH, Wiesbaden, Germany) were used in this study. The foams were supplied in large plates 8 mm in thickness and were cut to size by punching with a metal stamp to cylinders of 12 mm in diameter. The tablets were then washed in 1 L deionised H_2O and 10 ml Deconex (Burer Chemie AG, Zuchwill, Switzerland) for 2 min, and subsequently in ethanol (Absolute, Arcus, Oslo, Norway). The tablets were then dried at room temperature for 24 h and stored in PE-bags.

Table 1
Heating intervals during sintering.

Sequence	Temperature range (°C)	Heating rate (K/min)	Duration (min)
1	25–450	0.5	850
2	450	0	60
3	450–1500	3	350
4	1500	0	360–3000
5	1500–50	6	242

The polymer foams were then dipped into the ceramic slurry, which then later were centrifuged (Biofuge 22R Heraeus Sepatech, Osterode, Germany) at 1500 rpm for 2 min at 18 °C. The samples were then placed onto a porous ceramic plate and dried at room temperature for at least 24 h prior to sintering. The burnout of the polymer and the sintering of the ceramic part were chosen followed a detailed schedule (Table 1) in sinter oven (HTC-08/16, Nabertherm GmbH, Bremen, Germany). Five different holding times (6, 10, 20, 30, 40 and 50 h) were investigated.

Some scaffolds were double coated scaffolds. After sintering, the scaffolds were dipped and centrifuged as previously described. These scaffolds were sintered to 1500 °C at a rate of 3 K/min. All scaffolds were weighed (Mettler AT261 DeltaRange, Greifensee, Switzerland) prior to further analysis.

2.3. Compressive strength of sintered TiO_2 scaffold

The mechanical strength of the scaffold was performed in a compression test (Zwicki, Zwick/Roell, Ulm, Germany) according to DIN EN ISO 3386 on a load cell of 200 N. The scaffold was preloaded with a force of 2 N. The speed of the compression was set to 100 mm/min.

2.4. Pore morphology of sintered TiO_2 scaffold

Optical observation of the scaffold was performed by SEM (Tabletop SEM, Hitachi, Japan) with back scattered secondary ions at 15 kV.

The scaffolds were analysed using a 1172 microCT imaging system (Skyscan, Aartselaar, Belgium) desktop X-ray CT scanner at 7 μm voxel resolution X-ray tube current 173 μA and voltage 60 kV with a 0.5 mm aluminium filter. Specimens were mounted vertically on a plastic support and rotated 180° around the long axis (z-axis) of the sample. Three absorption images were recorded every 0.300° of rotation. These projection radiographs of scaffolds were first reconstructed to serial coronal-oriented tomograms using a 3D cone beam reconstruction algorithm. The beam hardening was set to 20% and ring artefact reduction to 12. 3D reconstruction of the internal pore morphology was carried out using these axial bitmap images and analysed by CTan and CTvol (Skyscan, Aartselaar, Belgium). A threshold analysis was then performed to determine the threshold value for which grayscale tomograms of scaffolds were most accurately represented by their binaries counterparts in terms of porosity. The grayscale threshold was set between 55 and 255. All objects smaller than 50 voxels and not connected to

the 3D model was removed prior to further analysis. In order to eliminate potential edge effects the cylindrical volume of interest (VOI) was selected in the center of a scaffold ($d = 2$ mm, $h = 3$ mm). Scaffold porosity was then calculated as:

$$\text{porosity} = 100\% - \text{vol.\% of binarised object in VOI} \quad (1)$$

All images underwent a 3D analysis, following by a "shrink-wrap" function, which allowed measuring fraction of the pore volume in a scaffold that was accessible from the outside through openings of a certain minimum size.[27] A shrink-wrap process was performed between two 3D measurements to shrink the outside boundary of the VOI in a scaffold through any openings whose size was equal to or larger than a threshold value (0–250 μm were used in this study). Interconnection was calculated as follows:

$$\text{interconnection} = \frac{V - V_{\text{shrink-wrap}}}{V - V_{\text{m}}} \times 100 \quad (2)$$

where V was the total volume of the VOI, $V_{\text{shrink-wrap}}$ was the VOI volume after shrink-wrap processing, and V_{m} was the volume of scaffold material.

The mean pore diameter distribution was found by measuring the material thickness on the inverse model, which was generated by setting grayscale threshold between 0 and 55. Noise was removed by despeckling any object smaller than 50 voxels and not connected to the 3D-body. The 3D models were generated through the algorithm adaptive rendering. The density of the scaffold strut was measured using the same software, and calibration was taken at 1.25 and 1.75 g/cm^3. The calibration from grayscale to density was performed to Hounsfield unit correction. This relationship was assumed linear.

Surface area was measured with the BET isotherm in liquid nitrogen (TriStar 3000, Micromeretics, Mönchengladbach, Germany). The crystallinity of the scaffolds was examined by X-ray diffraction (XRD) collected with a diffractometer in reflection mode (Cu Kα1 radiation; Ge monochromator; Braun position-sensitive detector Siemens D5000, Munich, Germany).

2.5. Determination of cytotoxicity of sintered TiO_2 scaffold

The mouse osteoblast cell line MC3T3-E1 (DSMZ, ACC210, Braunschweig, Germany) was routinely cultured at 37 °C in humidified atmosphere of 95% air and 5% CO_2 and maintained in alpha-MEM (PAA Laboratories Gmbh, Austria) supplemented with 10% fetal calf serum (PAA Laboratories Gmbh, Pasching, Austria), 100 U/ml penicillin, and 0.1 mg/ml streptomycin (PAA Laboratories Gmbh). For the assay, scaffolds were placed in the 24-well plated, cells were plated at densities of 0.25×10^6 cells in 500 μl of culture media on the surface of scaffolds and tissue cell culture dish.

Cytotoxicity responses of osteoblast cells were assessed by measurements of lactate dehydrogenase (LDH) release from necrotic cells into the culture media after days 1, 2, and 3. The LDH was measured by LDH Cytotoxicity Detection kit (Boehringer, Mannheim, Germany) according to manufactures' protocol using 50 μl of sample. Culture medium without cells was used as a zero absorbance to calibrate the spectrophotometer. The relative LDH released was expressed as a percentage of LDH to totally lysed cells with 1% Triton X-100 detergent.

Table 2
Variations in zeta potential at different pHs with standard deviation ($n = 5$).

pH	Average zeta potential (mV)	S.D.
1.5	43.1	3.5
1.7	44.4	1.9
1.9	55.4	3.9
2.2	36.5	0.9
2.4	37.9	0.7
2.6	27.3	1.1

The scaffolds were then fixed in 4% paraformaldehyde (PFA) and dehydrated by a graded ethanol (Merck, Darmstadt, Germany) series from 10 to 100%, with three times 10-min incubation at each step. Dehydration was then completed by critical point drying using CO_2 (CPD-030, Bal-Tec AG, Balzers, Liechtenstein). The scaffolds were gold sputtered (MACHINE) and examined in SEM (Tabletop SEM, Hitachi, Japan) with back scattered secondary ions at 15 kV.

2.6. Statistics

Batch variations were analysed by comparing the standard deviation of four randomized scaffolds from 16 different batches. Different data groups were compared through a two-tailed ANOVA test, where the significant level was set at 0.05. A correlation study was performed with a bivariate regression analysis, Spearman two-tailed, using the computer software Statistical Package for Social Sciences (SPSS) version 17.0 for Windows. The results were interpreted as follows: no correlation if $|r| < 0.3$, correlation if $0.3 < |r| < 0.5$, and strong correlation if $0.5 < |r| < 1$.[28] A negative r indicated a negative correlation while a positive r indicated a positive correlation.

3. Results

3.1. Slurry preparation

The maximum zeta potential was found at pH 1.9 (Table 2). An optimal particle size distribution was obtained from jacket-cooled blade rotator for the duration of 5.5 h (Fig. 1). Particle size distribution showed that 99% of the particles had the maximum size in a variety range of 0.48–0.84 μm. The bead mill and planetary mill did not provide the required particle size distribution. Slurry with high viscosity (>73 wt.% TiO_2) produced scaffolds with closed pores, while slurry with low viscosity (<60 wt.% TiO_2) coated polymer templates unevenly. A solid content around 68 wt.% TiO_2 provided the most favourable sponge loading.

3.2. Sintering

The results from the XRD measurement of the anatase powder and sintered scaffolds are presented in Fig. 2. The diffraction signals are displayed from 15° to 85°. The relative intensity was

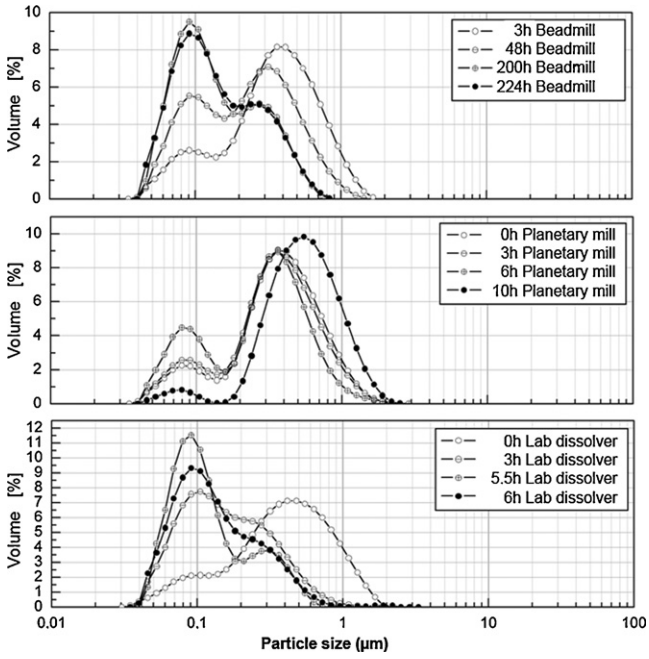

Fig. 1. Milling procedures for beadmill, planetary mill and lab dissolver. The most effective procedure was 5.5 h of lab dissolver.

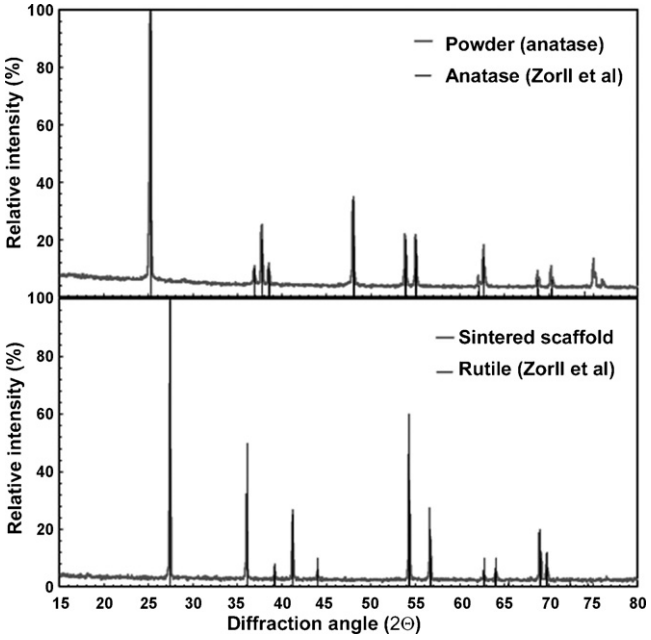

Fig. 2. XRD pattern of powder prior to sintering (top) and scaffold after sintering. The sintered scaffolds fit well with published XRD data for rutile structures 29.

taken from the main peak.[29] XRD data for anatase and rutile titanium oxide structures are also presented in Fig. 2. The anatase structure fits well with the starting powder and the rutile structure fits well with the sintered scaffolds. Thus, the current sintering process produced rutile titanium oxide crystalline structure.

The polymer sponge templating method left a hollow space inside the ceramic strut after sintering. When temperature of 1500 °C was held for longer than 30 h, this hollow space collapsed (Fig. 3B).

3.3. Scaffold characterization

The porosity of the scaffolds in this study had a maximum value of 96.5% and a lower value of 76.4%. The variation in porosity for each batch was 1.4% ($n = 168$). The strut diameter maximum thickness was found to be 113.1 μm, the minimum diameter was 30 μm and average value of 33.8 μm (S.D. ±5.7 μm). The mean pore diameter was 530.5 ± 30.9 μm, with 461.5 μm as the smallest pore and 747.7 μm as the largest. Fragmentation index for strut and fragmentation index for pore both had a negative value with an average of −0.013 μm (S.D. ±0 μm) for the former and an average value of −0.010 μm (S.D. ±0.003 μm) for the latter. The average value of anisotropy of the pore was 1.57 (S.D. ±0.32 deviation). The fractal dimension for the strut was calculated to 2.03 (S.D. ±0.03 (Table 3)). The mean density was measured to an average of 2.74 g/cm^3 (S.D. ±0.05 g/cm^3). The mean pore size was 530 μm. The mean strut size increased from 28

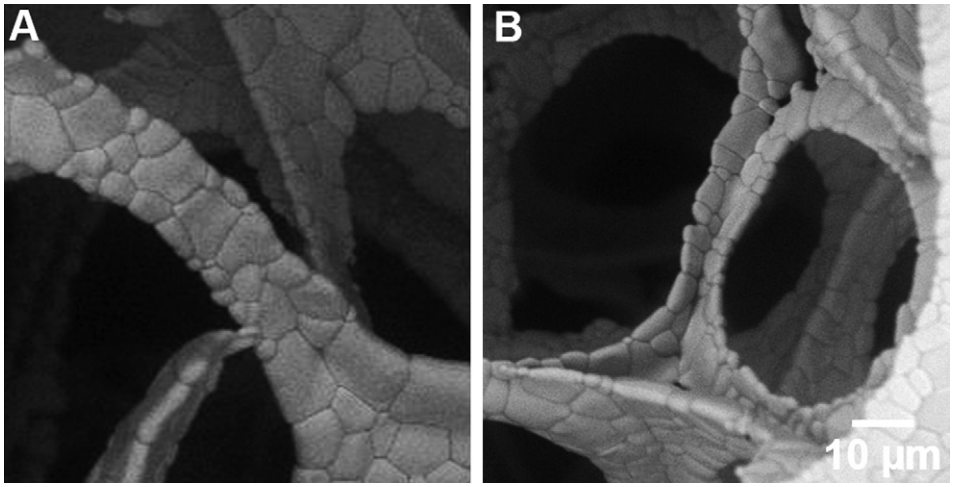

Fig. 3. (A) This strut has not collapsed due to a too short holding time, <30 h. (B) A wall of the three-sided strut has collapsed removing the former hollow space inside when the holding time at 1500 °C exceeds 30 h.

Table 3
Selected parameters from 3D μCT analysis displaying minimum, maximum, average values ($n = 68$) and standard deviation compiled from 16 different batches.

Parameter	Unit	Min.	Max.	Average	S.D./batch
Porosity	%	76.4	96.5	85.6	0.6
Interception surface	μm^2	9.1E+05	7.3E+08	2.6E+07	8.6E+07
Interception/object surface	μm^2	0.004	3.163	0.358	0.604
Object surface/volume ratio	1/μm	0.040	0.133	0.100	0.008
Strut diameter thickness	μm	30.0	113.1	33.8	5.7
Pore diameter thickness	μm	461.5	747.7	530.5	30.9
Structure linear density	1/μm	0.001	0.002	0.001	0.000
Fragmentation index strut	1/μm	−0.031	−0.006	−0.013	0.003
Fragmentation index pore	1/μm	−0.025	0.002	−0.010	0.003
Structure model index strut	SMI	−0.48	2.78	0.06	0.45
Structure model index pore	SMI	−11.20	1.80	−6.14	1.49
Degree of anisotropy strut	DA	0.000	2.16	1.17	0.23
Degree of anisotropy pore	DA	0.000	3.05	1.57	0.32
Fractal dimension strut		2.09	2.35	2.03	0.03
Fractal dimension pore		2.01	2.14	1.88	0.01
Mean density	g/cm^3	2.79	3.44	2.74	0.05

to 45 μm by multiple coating. The strut sizes also exposed a broader size distribution range for multiple coated scaffolds where the distribution increased from 10–60 to 10–110 μm (Fig. 6).

The pore structure was found to be open (Fig. 4A). The inner space of the scaffold was also found to be open porous (Fig. 4B), as can be viewed in a 3D animation (see Electronic Annex 1 in the online version of this article). When measuring the interconnection in the μCT (shrink-wrap mode), the scaffolds were found to have high numbers of interconnecting pores (Fig. 7). The interconnection was slightly changed by multiple coating, where a reduction of less than 5% was observed between the quadruple and double coated scaffold. The mean interconnection was reduced at most 9% from a minimum connective pore size of 250 μm. The single coated scaffold showed 15% mean reduction for its interconnection from a minimum connective pore size of 250 μm (Fig. 7).

3.4. Mechanical strength versus scaffold characterization

Several processing parameters were correlated against compressive strength (Table 4). The strength was found to correlate strongly with scaffold weight ($r = 0.777$, $p = 0.0004$), number of coating ($r = 0.526$, $p = 0.0007$) and cumulative sinter

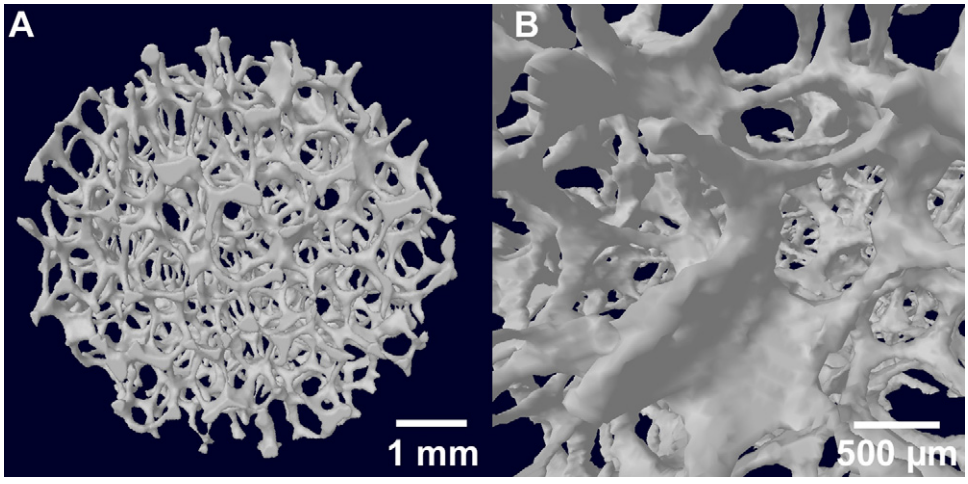

Fig. 4. μCT 3D image of a open porous TiO_2 scaffold (A) and close-up image from inside the same scaffold (B).

Table 4
Correlation study between compressive strength and coating parameters ($n = 160$).

Spearman's correlation coefficient	Solid content in slurry (wt.%)	Holding time (h)	Cumulative sinter hours (h)	Scaffold's weight (g)	Number of coating
Compressive strength (MPa)	−.142**	.208**	.560**	.777**	.526**

** $p < 0.01$.

Table 5
Correlation study between micro CT analysis and compressive strength ($n = 147$, $^{**}p < 0.01$).

Spearman's correlation coefficient	Porosity (%)	Strut size (μm)	Pore size (μm)	Fractal dimension strut	Mean density (g/cm^3)	Object surface/ volume ratio (%)
Compressive strength (MPa)	−.626**	.428**	−.180**	.394**	.534**	−.588**

** $p < 0.01$.

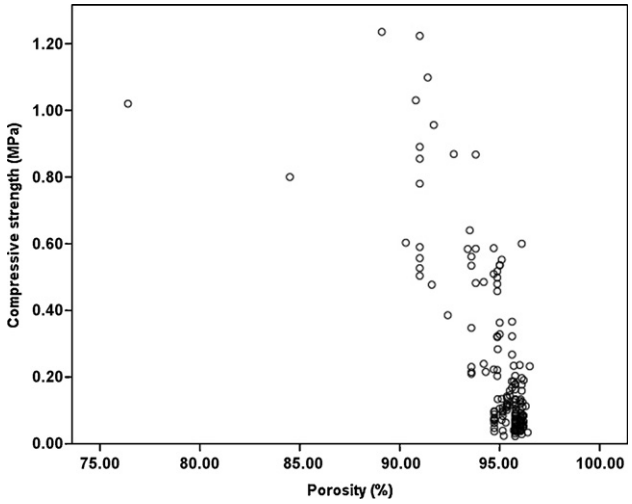

Fig. 5. Dot plot showing compressive strength against porosity.

hours ($r = 0.560$, $p = 0.001$). No or low correlation was found when comparing compressive strength to solid content in slurry ($r = -0.142$, $p = 0.001$), and holding sinter time ($r = 0.208$, $p = 0.0005$).

The pore structure of the scaffolds was analysed with micro CT and correlated with compressive strength. Porosity was strongly correlated to strength ($r = -0.626$, $p = 0.0008$) (Table 5). The scaffold with lowest porosity provided the highest mechanical strength (Fig. 5). Strong correlation was also found with object surface/volume ratio ($r = -0.588$, $p = 0.0006$), mean density ($r = 0.534$, $p = 0.0009$), strut size ($r = 0.428$, $p = 0.0005$), and the fractal dimension ($r = 0.394$, $p = 0.0001$). No correlation was found with pore size alone ($r = -0.180$, $p = 0.006$) (Table 5).

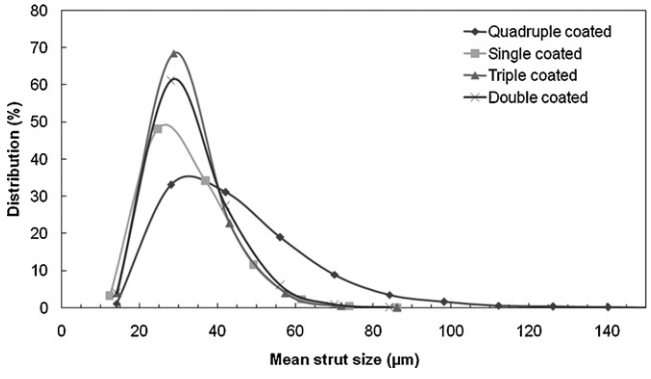

Fig. 6. Changes in mean pore strut size of the scaffold dependent on number of coating.

3.5. Surface structure

The BET surface area was found to be 5.06 m^2/g. The titanium oxide scaffold surface had an isotropic nanostructured surface which is shown in Fig. 8B. This wavelike structure covered the entire grains (Fig. 8A). Profilometer images (Fig. 8C) quantified this pattern. The latter method was used to measure the surface roughness; the result is displayed in Fig. 8B. The surface roughness, S_a, on the titanium oxide scaffolds was 890 ± 420 nm, and the root mean square, S_q, 1.12 ± 0.56 μm (Table 6). Skewness, S_{sk}, is a topographical parameter that describes the amount of valley and/or peaks on a surface. If S_{sk} is greater than 0, there are more valleys than peaks and *vice versa*. Since S_{sk} here was -0.87 ± 0.31 μm, there are slightly more valleys than peaks on the ceramic surface. The kurtosis, S_{ku}, 3.28 ± 0.79 μm revealed that the peaks are steep. The fractal number, S_{fd}, 2.35 ± 0.06 showed that the surface was complex and the fluid retention number, S_{ci}, measured to 0.53 ± 0.26 was within a range which has been positively correlated with bone attachment.[30]

3.6. Cytotoxicity

The LDH assay showed that the titanium oxide scaffolds were not cytotoxic (Fig. 9). Cytotoxic was significantly lower than the control (tissue culture plastic) ($p < 0.01$). Mouse osteoblasts adhered well to the scaffold surface and were evenly spread throughout the entire scaffold. The osteoblasts showed typical

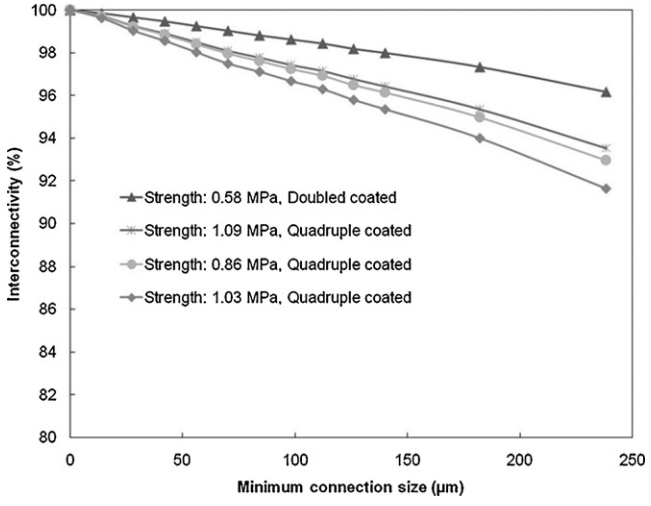

Fig. 7. Interconnection of the titanium oxide scaffold versus minimum pore connection size, which shows that the scaffolds are very well interconnected. Number of coating reduces the interconnection by less than 5%.

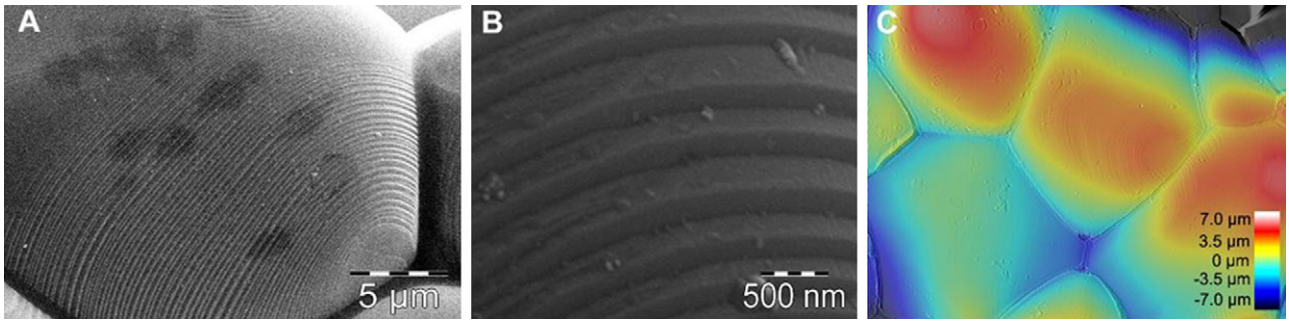

Fig. 8. SEM image of the surface of a titanium oxide scaffold (A), the same surface but with higher magnification (B) and profilometer image (C).

Table 6
Surface characterization parameters of the titanium oxide scaffold ($n = 5$).

Surface parameters					
S_a (μm)	S_q (μm)	S_{sk}	S_{ku}	S_{fd}	S_{ci}
0.89 ± 0.42	1.12 ± 0.56	−0.87 ± 0.31	3.28 ± 0.79	2.35 ± 0.06	0.53 ± 0.26

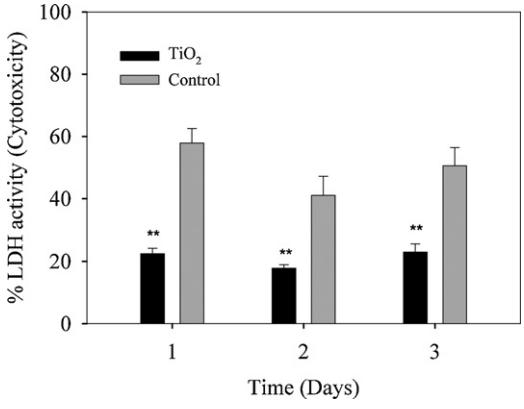

Fig. 9. Cytotoxicity measurement of the titanium oxide scaffolds compared to control (tissue culture plastic). The cytotoxicity of titanium scaffolds were significantly lower than tissue culture dish (**$p < 0.01$) at all three different time points. Error bars are standard error of the mean ($N = 8$).

morphology and were even stretched from strut to strut, as the SEM image after 3 days of incubation shows (Fig. 10).

4. Discussion

4.1. Coating procedures

Manufacture of mechanical loadable scaffolds requires optimal slurry for impregnation of the replica foam. Slurry with high viscosity (>73 wt.% TiO_2) produced scaffolds with more closed pores, while slurry with low viscosity (<60 wt.% TiO_2) gave unevenly coated polymer templates. A solid content between 60 and 70 wt.% TiO_2 provided most favourable sponge coating. Similar results have been found in other studies when using the polymer sponge method with Al_2O_3 slurries.[31,32] The solid content in the slurry in our study did not positively correlate with the mechanical strength of the scaffold, but was found to be crucial in terms of providing an open porosity.

Sintering is an energy driven mechanism, and it seemed that a holding time of more than 30 h at 1500 °C provided enough energy for the collapse of the hollow strut. This phenomenon has not been reported previously, although it has been reported that the stress–strain responses of ceramic foams made by sponge-replication show isotropy and strain rate dependence. The weakest part of a framework is the brittleness of the strut shape, which caused the initiation and expanding of cracks.[33] Here we found, that the brittleness of the struts was greatly reduced, after a holding time more of than 30 h. Holding temperature procedure at 1500 °C during sintering should thus exceed 30 h to obtain a strut-folding. Pictures taken with SEM showed strut collapsing after 30 h, which made the struts stronger as the hollow space inside diminished, leaving a compact structure instead of a hollow one with weak area. These findings were verified by the Spearman correlation study (Table 5), where there was found a correlation ($r = 0.394$) between increase in the struts' fractal number and its compressive strength. Struts

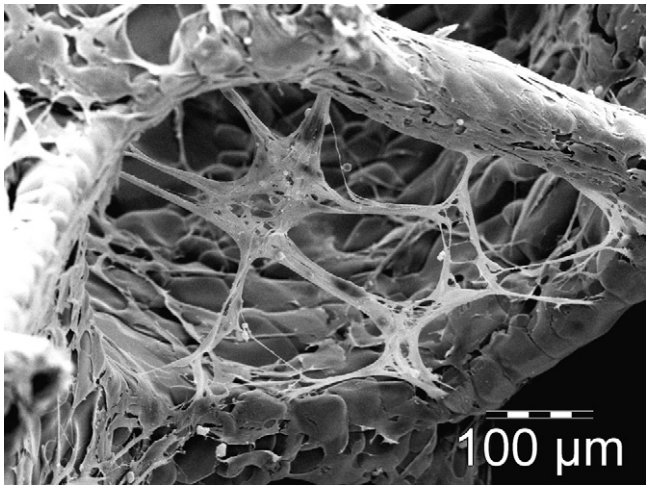

Fig. 10. SEM image of osteoblasts which had adhered and spread onto the scaffold surface after 3 days of incubation.

that had collapsed also exhibited a higher fractal numbers indicating a more irregular shape. Unexpectedly, this correlation was weaker compared to both porosity and strut size. This phenomenon is mostly likely due to the fact that 95% of the produced scaffolds were sintered longer than 30 h, and that the effect of the holding time is not truly represented.

According to the correlation study the most effective way to mechanical strengthen the scaffold, was to increase the strut size, as previously reported by Min et al.[34] Increase in strut size and decrease in porosity were the two strongest prevailing parameters in the correlation study (Table 5). The strategy of increasing the strength of scaffolds produced by the polymer foam method has previously been carried out by multiple coatings.[35,36] The thickness of the struts also increased with number of slurry coating and resulted in stronger scaffold with an increase in compressive strength.

4.2. Scaffold characterization

The reproducibility of the polymer sponge method was found to be sufficient. The morphological parameters had low standard deviation (Table 3), e.g. the standard deviation (per batch) for porosity was ±1.6% and ±30.9 μm for pore size.

High porosity and large pore diameter optimize the conditions for osseoconductivity and vascular ingrowth in scaffold. Optimal pore size is believed to about 300 μm,[37] with a porosity higher than 70%.[38,39] The scaffolds produced in the present study had an average pore size of 582.07 μm and a porosity of 94.3% which allow for further slurry coatings and subsequently improved strength, while still maintaining favourable conditions for osseoconductivity and vascular ingrowth.

The pore interconnection was found to be very high in comparison to other commercially available scaffolds characterised in the same matter. A study performed by Shi et al.[40] showed a scaffold with accessible porosity range at maximum 75% for a minimum pore connection size of 200 μm. Hacker et al.[41] reported up to 50% reduction of the interconnection with the same minimum pore connection size. Our scaffolds had an accessible of porosity maximum 98% for this minimum pore connection size. Having found a decrease in interconnection for the multiple coated scaffolds (Fig. 7), this reduction was most likely due to the increase in strut size which was seen in Fig. 6.

4.3. Mechanical strength

Earlier reported TiO_2 scaffolds have had limited ability of bearing the loads at the implant site. Compression strength of trabecular bone has been reported to be in the range of 0.5–12 MPa.[42] The TiO_2 scaffolds in the present study had a compressive strength up to 1.2 MPa. These scaffolds had a porosity of 90%, which is higher than necessary for a successful scaffold. However, in comparison with other bioactive ceramic scaffolds (tri-calcium phosphates) the TiO_2 scaffolds reported have superior mechanical strength.[42–44] The correlation between mechanical strength and cumulative sinter hours can be explained by the fact that multiple sintering sequencing also means multiple coating cycles, as the correlation factor is almost identical. Applying thicker layers of ceramic on the polymer scaffold and thus making the scaffold more dense (75%) would probably also improve the scaffolds' mechanical properties.

5. Conclusion

This study has showed that it is possible to repeatedly manufacture ultra-porous TiO_2 scaffolds that have the strength of trabecular bone. TiO_2 scaffolds with porosity as high as 90%, high interconnection and with a compressive strength exceeding 1.2 MPa have routinely been made. No other studies with scaffolds made from bioactive ceramics have been reported with equally high compressive strength and at the same time having an average porosity above 90%. Since the porosity is far above what is recommendable for osseointegration, a reduction of porosity would reinforce the scaffolds' strength even further. The correlation study defined the most important manufacturing steps and the governing morphological characteristics for increased mechanical strength. The key manufacturing factors were multiple coatings of the scaffold in the slurry and holding sintering time above 30 h at 1500 °C. The cytotoxicity assay showed that the titanium oxide scaffolds were less cytotoxic than tissue culture plastic. Mouse osteoblasts adhered well to the scaffold surface and were evenly spread throughout the entire scaffold (Ø = 8 mm).

Acknowledgements

The authors would like to thank Tove Larsen, School of Pharmacy, University of Oslo for kind assistance during zeta potential measurements and Dr. Phil Salmon, SkyScan for excellent consulting during the μCT analysis. This study was supported by a grant from the Norwegian Research Council, Grant number 171058.

Appendix A. Supplementary data

Supplementary data associated with this article can be found, in the online version, at doi:10.1016/j.jeurceramsoc.2009.03.017.

References

1. Torres, F. G., Nazhat, S. N., Sheikh Md Fadzullah, S. H., Maquet, V. and Boccaccini, A. R., Mechanical properties and bioactivity of porous PLGA/TiO_2 nanoparticle-filled composites for tissue engineering scaffolds. *Compos. Sci. Technol.*, 2007, **67**, 1139–1147.
2. Stock, U. A. and Vacanti, J. P., Tissue engineering: current state and prospects. *Annu. Rev. Med.*, 2001, **52**, 443–451.
3. Lancet, T., Legal and illegal organ donation. *The Lancet*, 1901, **369**.
4. Chen, Q.-Z., Rezwan, K., Francon, V., Armitage, D., Nazhat, S. N., Jones, F. H. *et al.*, Surface functionalization of bioglass(R)-derived porous scaffolds. *Acta Biomater.*, 2007, **3**, 551–562.
5. Cheung, H.-Y., Lau, K.-T., Lu, T.-P. and Hui, D., A critical review on polymer-based bio-engineered materials for scaffold development. *Comp. B: Eng. Bio-Eng. Comp.*, 2007, **38**, 291–300.
6. Chim, H., Hutmacher, D. W., Chou, A. M., Oliveira, A. L., Reis, R. L., Lim, T. C. *et al.*, A comparative analysis of scaffold material modifications for

load-bearing applications in bone tissue engineering. *Int. J. Oral Maxillofac. Surg.*, 2006, **35**, 928–934.
7. Lickorish, D., Guan, L. and Davies, J. E., A three-phase, fully resorbable, polyester/calcium phosphate scaffold for bone tissue engineering: evolution of scaffold design. *Biomaterials*, 2007, **28**, 1495–1502.
8. Rezwan, K., Chen, Q. Z., Blaker, J. J. and Boccaccini, A. R., Biodegradable and bioactive porous polymer/inorganic composite scaffolds for bone tissue engineering. *Biomaterials*, 2006, **27**, 3413–3431.
9. Wang, H., Li, Y., Zuo, Y., Li, J., Ma, S. and Cheng, L., Biocompatibility and osteogenesis of biomimetic nano-hydroxyapatite/polyamide composite scaffolds for bone tissue engineering. *Biomaterials*, 2007, **28**, 3338–3348.
10. Thomson, R. C., Shung, A. K., Yaszemski, M. J. and Mikos, A. G., Scaffold processing. In *Principles of Tissue Engineering*, ed. R. Lanza, R. Langer and J. Vacanti. Academic Press, San Diego, 2000, pp. 252–259.
11. Bose, S., Darsell, J., Kintner, M., Hosick, H. and Bandyopadhyay, A., Pore size and pore volume effects on alumina and TCP ceramic scaffolds. *Mater. Sci. Eng. C*, 2003, **23**, 479–486.
12. Brunski, J. B., Ratner, B. D., Hoffman, A. S. and Schoen, F. J. *et al.*, ed., *Biomaterials Science: An Introduction to Materials in Medicine*. Academy Press, New York, 1996, pp. 37–50.
13. Jones, J. R. and Hench, L. L., Regeneration of trabecular bone using porous ceramics. *Curr. Opin. Solid State Mater. Sci.*, 2003, **7**, 301–307.
14. Crane, G. G. M., Ishaug, S. S. L. and Mikos, A. A. G., Bone tissue engineering. *Nat. Med.*, 1995, **1**, 1322–1324.
15. Jokinen, M., Pätsi, M., Rahiala, H., Peltola, T., Ritala, M. and Rosenholm, J. B., Influence of sol and surface properties on in vitro bioactivity of sol–gel-derived TiO_2 and TiO_2–SiO_2 films deposited by dip-coating method. *J. Biomed. Mater. Res.*, 1998, **42**, 295–302.
16. Rincon, A.-G. and Pulgarin, C., Bactericidal action of illuminated TiO_2 on pure *Escherichia coli* and natural bacterial consortia: post-irradiation events in the dark and assessment of the effective disinfection time. *Appl. Catal. B: Environ.*, 2004, **49**, 99–112.
17. Yuranova, T., Rincon, A. G., Pulgarin, C., Laub, D., Xantopoulos, N., Mathieu, H.-J. *et al.*, Performance and characterization of Ag–cotton and Ag/TiO_2 loaded textiles during the abatement of *E. coli*. *J. Photochem. Photobiol. A: Chem.*, 2006, **181**, 363–369.
18. Zardiackas, L. D., Parsell, D. E., Dillon, L. D., Mitchell, D. W., Nunnery, L. A. and Poggie, R., Structure, metallurgy, and mechanical properties of a porous tantalum foam. *J. Biomed. Mater. Res.*, 2001, **58**, 180–187.
19. Peroglio, M., Gremillard, L., Chevalier, J., Chazeau, L., Gauthier, C. and Hamaide, T., Toughening of bio-ceramics scaffolds by polymer coating. *J. Eur. Ceram. Soc.*, 2007, **27**, 2679–2685.
20. Kaufman, J. D., Song, J. and Klapperich, C. M., Nanomechanical analysis of bone tissue engineering scaffolds. *J. Biomed. Mater. Res. Part A*, 2007, **81A**, 611–623.
21. Cesarano, J., Dellinger, J. G., Saavedra, M. P., Gill, D. D., Jamison, R. D., Grosser, B. A. *et al.*, Customization of load-bearing hydroxyapatite lattice scaffolds. *Int. J. Appl. Ceram. Technol.*, 2005, **2**, 212–220.
22. Kim, H. W., Knowles, J. C. and Kim, H. E., Development of hydroxyapatite bone scaffold for controlled drug release via poly(epsilon-caprolactone) and hydroxyapatite hybrid coating. *J. Biomed. Mater. Res. Part B: Appl. Biomater.*, 2004, **70B**, 240–249.
23. Dellinger, J. G., Wojtowicz, A. M. and Jamison, R. D., Effects of degradation and porosity on the load bearing properties of model hydroxyapatite bone scaffolds. *J. Biomed. Mater. Res. Part A*, 2006, **77A**, 563–571.
24. Baksh, D., Davies, J. E. and Kim, S., Three-dimensional matrices of calcium polyphosphates support bone growth in vitro and in vivo. *J. Mater. Sci. Mater. Med.*, 1998, **9**, 743–748.
25. Haugen, H., Will, J., Kohler, A., Hopfner, U., Aigner, J. and Wintermantel, E., Ceramic TiO_2-foams: characterisation of a potential scaffold. *J. Eur. Ceram. Soc.*, 2003, **24**, 661–668.
26. Schwartzwalder, K., Somers, A. V., Method of Making a Porous Shape of Sintered Refractory Ceramic Articles. *United States Patent No. 3,090,094* (1963).
27. Moore, M. J., Jabbari, E., Ritman, E. L., Lu, L. C., Currier, B. L., Windebank, A. J. *et al.*, Quantitative analysis of interconnectivity of porous biodegradable scaffolds with micro-computed tomography. *J. Biomed. Mater. Res. A*, 2004, **71A**, 258–267.
28. Cohen, J., *Statistical Power Analysis for the Behavioral Sciences* (*2nd ed.*). Lawrence Erlbaum Associates, New York, 1988, pp. 85–97.
29. Winkler, J., *Die Technologie des Beschichtens*. Vincentz Network, Berlin, 2003, pp. 23–25.
30. Lamolle, S. F., Monjo, M., Lyngstadaas, S. P., Ellingsen, J. E. and Haugen, H. J., Titanium implant surface modification by cathodic reduction in hydrofluoric acid: surface characterization and in vivo performance. *J. Biomed. Mater. Res. A*, 2008.
31. Montanaro, L., Jorand, Y., Fantozzi, G. and Negro, A., Cer foams by powder processing. *J. Eur. Ceram. Soc.*, 1998, **18**, 1339–1350.
32. Acchar, W., Ramalho, E. G., Souza, F. B. M., Torquato, W. L., Rodrigues, V. P. and Innocentini, M. D. M., Characterization of cellular ceramics for high-temperature applications. *J. Mater. Sci.*, 2008, **43**, 6556–6561.
33. Zhang, J. Y., Fu, Y. M. and Zeng, X. M., Compressive properties of open-cell ceramic foams. *Trans. Nonferr. Met. Soc. China*, 2006, **16**, 453–456.
34. Min, S. H., Jin, H. H., Jun, B. S., Park, I. M., Park, H. C. and Yoon, S. Y., Effect of reaction conditions on pore configuration and mechanical property for porous hydroxyapatite prepared by polymer sponge method. *High-Perform. Ceram. Part IV*, 2007, **336–338**(Pts 1–3), 1567–1570.
35. Kim, H. W., Lee, S. Y., Bae, C. J., Noh, Y. J., Kim, H. E., Kim, H. M. *et al.*, Porous ZrO_2 bone scaffold coated with hydroxyapatite with fluorapatite intermediate layer. *Biomaterials*, 2003, **24**, 3277–3284.
36. Kim, H. W., Kim, H. E., Salih, V. and Knowles, J. C., Dissolution control and cellular responses of calcium phosphate coatings on zirconia porous scaffold. *J. Biomed. Mater. Res. A*, 2004, **68A**, 522–530.
37. Karageorgiou, V. and Kaplan, D., Porosity of 3D biomaterial scaffolds and osteogenesis. *Biomaterials*, 2005, **26**, 5474–5491.
38. Byrne, D. P., Lacroix, D., Planell, J. A., Kelly, D. J. and Prendergast, P. J., Simulation of tissue differentiation in a scaffold as a function of porosity, Young's modulus and dissolution rate: application of mechanobiological models in tissue engineering. *Biomaterials*, 2007, **28**, 5544–5554.
39. Whang, K., Healy, K. E., Elenz, D. R., Nam, E. K., Tsai, D. C., Thomas, C. H. *et al.*, Engineering bone regeneration with bioabsorbable scaffolds with novel microarchitecture. *Tissue Eng.*, 1999, 5.
40. Shi, X., Sitharaman, B., Pham, Q. P., Liang, F., Wu, K., Edward Billups, W. *et al.*, Fabrication of porous ultra-short single-walled carbon nanotube nanocomposite scaffolds for bone tissue engineering. *Biomaterials*, 2007, **28**, 4078–4090.
41. Hacker, M., Ringhofer, M., Appel, B., Neubauer, M., Vogel, T., Young, S. *et al.*, Solid lipid templating of macroporous tissue engineering scaffolds. *Biomaterials*, 2007, **28**, 3497–3507.
42. Jones, J. R., Ehrenfried, L. M. and Hench, L. L., Optimising bioactive glass scaffolds for bone tissue engineering. *Biomaterials*, 2006, **27**, 964–973.
43. Wei, J., Chen, Q. Z., Stevens, M. M., Roether, J. A. and Boccaccini, A. R., Biocompatibility and bioactivity of PDLLA/TiO_2 and PDLLA/TiO_2/Bioglass(R) nanocomposites. *Mater. Sci. Eng. C*, 2008, **28**, 1–10.
44. Zhang, F., Lin, K., Chang, J., Lu, J. and Ning, C., Spark plasma sintering of macroporous calcium phosphate scaffolds from nanocrystalline powders. *J. Eur. Ceram. Soc.*, 2008, **28**, 539–545.